Operation analysis and parameter optimization of the conveying device for uniform crushed straw throwing and seed-sowing machines

Fengwei Gu[1,2], Youqun Zhao[1], Zhichao Hu[2], Lili Shi[2*], Feng Wu[2], Hongbo Xu[2], Xuemei Gao[2]

(1. *College of Energy and Power Engineering, Nanjing University of Aeronautics and Astronautics, Nanjing 210016, China*;
2. *Nanjing Institute of Agricultural Mechanization, Ministry of Agriculture and Rural Affairs, Nanjing 210014, China*)

Abstract: Uniform crushed straw throwing and seed-sowing machines can achieve the processes of straw chopping, straw transport, sowing, fertilization, and straw mulching at the same time, which is widely used in many areas of China. Conveying device is one of the important components used to convey, elevate and throw straw. However, the problems of high power consumption and congestion affect the promotion of the machine. Therefore, the conveying device of uniform crushed straw throwing and seed-sowing machine was analyzed in order to determine its device operation mechanism. Kinematic and dynamic analyses of particles of crushed rice straw during lifting and dispersion are used to develop a flexible-body model of rod-shaped and agglomerate-shaped crushed straw and a coupling model including the mechanical structure of the device. By integrating computational fluid dynamics and the discrete element method, the gas-solid coupling theory in numerical simulations and motion analysis of crushed straw particles is used to determine how the flow field and motion characteristics affect the conveying performance. Besides, regression equations to describe the relationships between the factors and each assessment index were established by using the regression analysis and response surface analysis with the software Design-Expert. The effect of throwing blade speed X_1, conveying volume of crushed straw X_2, and pipeline diameter X_3 on the throwing speed of crushed straw Y_1 and specific power consumption Y_2 were investigated. The highest throwing speed of crushed straw and lowest specific power consumption are the optimization goal .The results of optimization showed that the predict the best optimal parameters were 2000 r/min throwing blade rotational speed, 1.4 kg/s conveying volume, and 220 mm pipeline diameter, the planter achieved a throwing speed of 12.2 m/s and specific power consumption of 9179 m^2/s^2. And then a field test verification was conducted. The planter achieved a throwing speed 12.4 m/s and specific power consumption 9070 m^2/s^2 while selecting the best optimal parameters. Thus, the optimal parameters can provide a high-performance operation and satisfy the actual operation requirements The results provide a theoretical basis and data support for seeding technology innovation and equipment optimization to ensure uniform crushed straw throwing in dense rice stubble fields.

Keywords: rice straw stubble, uniform crushed straw throwing, coupled CFD-DEM, response surface analysis
DOI: 10.25165/j.ijabe.20231606.7057

Citation: Gu F W, Zhao Y Q, Hu Z C, Shi L L, Wu F, Xu H B, et al. Operation analysis and parameter optimization of the conveying device for uniform crushed straw throwing and seed-sowing machines. Int J Agric & Biol Eng, 2023; 16(6): 28–36.

1 Introduction

Currently, the total return and fertilizer are the most typical applications for the effective use of rice straw. High-quality and smooth machine-planting of wheat with rice stubble depends on synergistically removing obstacles and returning rice straw[1-3]. However, the worldwide development of no-till farming technologies mainly focuses on partially eliminating obstacles for straw through methods such as installing auxiliary diversion devices (e.g., straw guiding rollers), using mowing wheels to remove straw, and adopting belt-sending rotary tillage to prevent clogging on the planting row. Such methods allow root stubble to be removed and are suitable when a small portion of the previous crop ahead has been crushed[4]. However, clogging and obstacles created by straw hinder the smooth operation in dense and hard stubble fields, where dried seeds and planting on trellises have become crucial problems. Furthermore, the straw from a preceding rice crop exists in large quantities, has a high moisture content, and is extremely tough[5-7]. Thus, the subsequent seeding of wheat in such fields presents limited efficiency owing to the narrow seeding distance of planting machines and a large number of furrow openers. Therefore, achieving high-quality and smooth seeding of wheat remains challenging[8,9].

To improve rice-wheat crop rotation, our research team developed an uniform crushed straw throwing and seed-sowing machine for dense fields of rice straw stubble. This planter can simultaneously perform straw crushing, horizontal-level straw conveying, crossover displacing, uniform throwing, and soil covering, thus synergistically removing obstacles related to straw clogging and performing the field return of crushed straw by throwing and spreading[10,11]. Nevertheless, the massive, humid, and strong straw from the previous rice crop easily leads to agglomeration and entanglement, causing an excessive or inadequate exit velocity at the outlet of the conveying pipeline, as well as clogging, possibly undermining the throwing uniformity[12,13]. Then, excessive straw coverage may appear in some areas of the

Received date: 2021-09-25 **Accepted date:** 2023-09-07
Biographies: **Fengwei Gu**, Associate Research Fellow, research interest: agricultural mechanization engineering, Email: gfwsll@163.com; **Youqun Zhao**, Professor, research interest: mechanical engineering, Email: yqzhao@nuaa.edu.cn; **Feng Wu**, Associate Research Fellow, research interest: agricultural mechanization engineering, Email: xuefeng_1223@163.com; **Hongbo Xu**, Assistant Professor, research interest: agricultural mechanization engineering, Email: xhbnjs@163.com; **Xuemei Gao**, Assistant Professor, research interest: agricultural mechanization engineering, Email: 591882839@qq.com.
***Corresponding author: Lili Shi**, Assistant Professor, research interest: agricultural mechanization engineering. Nanjing Institute of Agricultural Mechanization, Ministry of Agriculture and Rural Affairs, Nanjing 210014, China. Tel: +86-15366092994, Email: 1301706961@qq.com.

working field, deteriorating the uniform heating and moisture preservation, as well as weed enclosure, and possibly leading to insufficient and weak seedlings in the subsequent wheat crop[14-16].

In this study, the planter operation mechanism for uniform crossways throwing of crushed rice straw and optimize the structural and operational parameters of key throwing components had been thoroughly characterized and analyzed. Consequently, a theoretical basis and data support are provided to address essential technical challenges to achieve uniform straw coverage and promote equipment research and development of seeding mechanization technologies in dense, hard stubble fields of rice straw.

2 Planter structure and operation analysis

2.1 Planter structure and operation

The crossways crushed straw throwing planter comprises a structure of a three-point suspension, as shown in Figure 1. This planter adopts the compact structure of rotary tillage for wheat seeding, and its rear part is equipped with integrated tubes for simultaneous deep fertilization and seed dropping while breaking the stubble. Moreover, the planter is equipped with adjustment components including straw pressing wheels and a supporting roller to adjust the straw height during crushing.

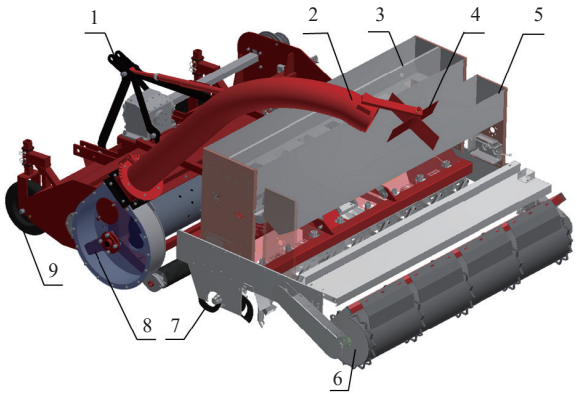

1. Traction frame 2. Pipeline 3. Fertilizer box 4. Dispersing impeller 5. Seed box 6. Straw pressing wheel 7. Straw crushing mechanism 8. Throwing blade 9. Support roller

Figure 1 Components of the developed planter

During operation, the planter first crushes the dense existing crop as a whole and collects the crushed straw. Subsequently, with strength and impact, the straw is lifted upwards along a conveying belt and thrown backwards across a wide range. As the straw is thrown crossways in the air, a seeding area without straw is formed underneath the planter, where the subsequent crop of wheat is fertilized and planted by rotary tillage and throwing.

Moreover, the machine presses the soil and uniformly spreads the crushed rice straw on the ground, completing the integrated operation while eliminating obstacles for straw collection, high-quality seeding, crushed straw spreading, as shown in Figure 2.

In this study, the motion of the crushed straw in the pipeline was focused to improve its conveying performance. The uniform spreading of crushed straw crossways involves rigid and flexible coupling interactions between the crushed straw and planter components. To identify and optimize the operation mechanism, a particle-agglomerate model should be derived based on the actual operation considering crushed straw agglomerates as the objects. By integrating this model into a 3D virtual simulation, the kinematic and dynamic characteristics of the rigid and flexible coupling models of the mechanism for crossways crushed straw throwing can be obtained and analyzed.

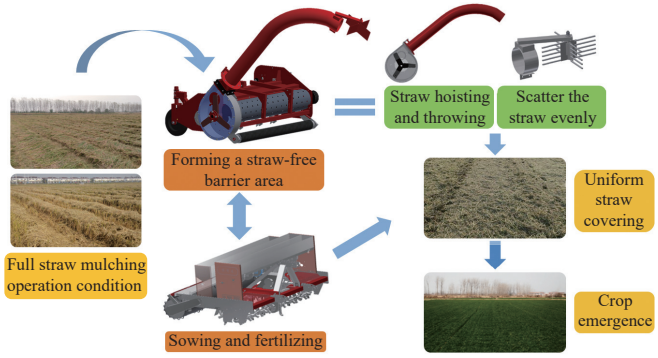

Figure 2 Diagram of crush and lifting crushed straw and dispersing process

3 Performance of the straw throwing mechanism

To better analyze the kinematic and dynamic characteristics of crushed straw throwing, the process was divided into the four stages illustrated in Figure 2: 1) throwing-lifting, 2) pneumatic crossing, 3) wall-pressure jetting, and 4) breaking down and spreading. After crushed straw enters the lifting and throwing device in agglomerates, it is thrown and lifted under the centrifugal force of the high-speed-rotation throwing blades. In the tilted two-section conveying pipeline, agglomerates of crushed straw are pushed crossways over the fertilizing, seeding, and soil pressing components by air force following a linear path. The agglomerates then depart after colliding with the arched wall, spraying backward and downward. After a final collision with the dispersing impeller, the agglomerates are broken down and scattered uniformly on the ground under the action of the rotating blow force, thus achieving crushed straw spreading.

According to Figure 3, crushed straw gains kinetic energy at the stage of conveying and transporting, which can contribute to the movement smoothness. In the absence of air resistance, the conveying capacity of throwing blades and the kinetic energy when the rice exists the throwing blades are given respectively as follows:

$$Q_t = 30n_t \cdot n \cdot \gamma \cdot \eta \cdot R^2 \cdot b_t \cdot \tan\varphi \tag{1}$$

$$E = \frac{1}{2}mv_a^2 - \frac{1}{2}m\rho_0^2\omega^2 \tag{2}$$

where, Q_t is conveying capacity of throwing blades, kg/h; n_t is rotational speed of throwing blades, r/min; n is the number of throwing blades; γ is per unit mass of conveyor, g; η is efficiency coefficient; R is radius of throwing blades, m; b_t is width of throwing blades; φ is natural repose angle of conveyor; v_a is absolute speed of crushed straw when leaving throwing blades, m/s.

The throwing blades of the crushed straw lifting and throwing device and the horizontal convey dragon are assembled coaxially, considering the transmission, so that the device performance is suitable for a throwing blade rotational speed between 1700 and 2300 r/min. The number of throwing blades is three, radial and circular, and redistributed uniformly. Moreover, a larger throwing blade diameter provides a smoother motion of the crushed straw and reduces the agglomeration while also increasing the straw throwing speed. Considering the power dissipation and field working condition, the internal diameter of throwing blades to were set to 0.6 m, the radius of throwing blades to 0.3 m, and the width of throwing blades to 0.145 m. From the lifting-throwing stage to the

pneumatic throwing stage, the speed of the straw is roughly the same of the wind speed. Thus, the following kinetic energy equation can be obtained:

$$E_0 = \frac{1}{2}mv_o^2 \tag{3}$$

where, E_0 is the steady kinetic energy when entering into conveying pipeline, J; m is the mass of crushed straw.

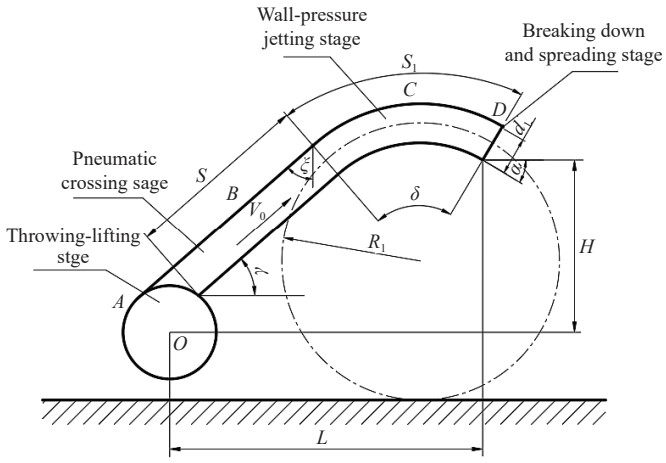

Note: L, H are the horizontal distance and the vertical distance between vane lifting and conveying device pivot point O and export of two-segment lifting conveying device, mm; S, S_1 are the pipeline section length and bent pipeline length of two section conveying pipelines, mm; γ is included angle between pipeline section of two-segment lifting conveying device and horizontal plane, (°); ξ is collision angle (°); α is included angle between export of two-segment lifting conveying device and horizontal plane, (°); R_1 is curvature radius of two-segment lifting conveying device bent pipeline, mm; δ is radian of two-segment lifting conveying device bent pipeline, (°). The rice straw's working process of straw transport device included four stages: lifting-throwing stage, pneumatic throwing stage, wall pressure jetting stage, and crushing-covering stage. A, B, C, D are four positions of rice straw in lifting conveying device. v_0 is the mean wind speed in the pipeline, m/s.

Figure 3 Geometric structural and working process diagram of straw transport device

Furthermore, the elastic scattering of the crushed straw on the curved pipeline of the conveying pipeline occurs immediately; thus, collision energy loss (ΔE) of crushed straw and bent pipeline can be written as follows:

$$\Delta E = \frac{1}{2}mv_o^2 \sin\xi \tag{4}$$

Subsequently, the slide crushed straw along the conveying pipeline is as follows:

$$F_e = F_f - F_t \tag{5}$$

where, F_e is force in the crushed straw slip on the curved pipeline of the conveying system, N; F_f is Friction in the crushed straw slip on the curved pipeline of the conveying pipeline, N; F_t is Air force in the crushed straw slip on the curved pipeline of the conveying pipeline, N.

$$F_t = CA\rho V_2^2/2 \tag{6}$$

where, A is windward projection area of crushed straw, m^2; ρ is air density, kg/m^3; V_2 is relative velocity between the crushed straw and the airflow velocity in the conveying pipeline, m/s; C is dimensionless factors.

$$\Delta E' = \int_0^{S_e} F_e \mathrm{d}S \tag{7}$$

where, $\Delta E'$ is Energy loss in the crushed straw slip on the curved pipeline of the conveying pipeline, J; S_e is total distance of the curved pipeline of the conveying pipeline, m; E_s is kinetic energy of the crushed straw:

$$E_s = E_0 - \Delta E - \Delta E' = \frac{1}{2}mv_0^2\cos\xi^2 - \int_0^{S_e} F_e \mathrm{d}S \tag{8}$$

To make sure crushed straw gain high kinetic energy when leaving throwing blades, it will reduce energy loss also. Throwing kinetic energy of crushed straw and average winds speed in the conveying pipeline are in the direct ratio. Throwing kinetic energy of crushed straw is in reverse ratio with collision angle ξ, bent pipeline length of two sections of conveying pipeline S_1.

Considering the real conditions such as power consumption and crushed straw movement state in conveying pipeline, research on computer simulation and field experiment are necessary.

4 Coupling simulation based on computational fluid dynamics and discrete element method

4.1 Mathematical models

Figures 4 and 5 show the dimensions and grid division diagram, respectively, of the crushed straw lifting and throwing device. To further determine the motion and trajectory of the crushed straw in this device, a simulation using a computational fluid dynamics/discrete element method (CFD-DEM) model of particle motion was conducted in order to analyze gas-solid coupling， aiming both to obtain the basic characteristics of the flow field and to quantitatively analyze the number of particle collisions, volume fraction, and distribution of gas velocity[17-19].

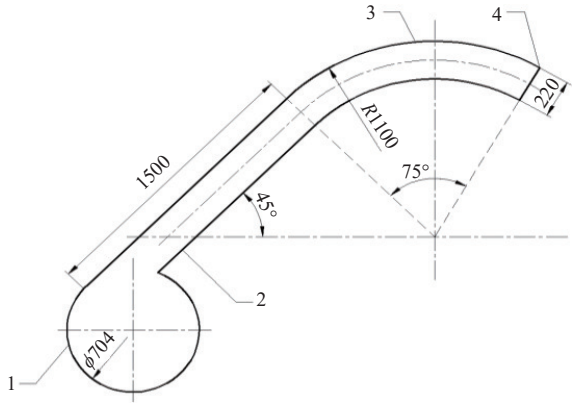

1. Pneumatic throwing device 2. Straight pipeline section 3. Bent pipeline section 4. Spout straw port.

Figure 4 Pipeline dimensions of crushed straw lifting and throwing device

Figure 5 Pipeline grid division diagram of crushed straw lifting and throwing device model

In the CFD-DEM coupling model, the reduced Navier-Stokes equation from computational fluid dynamics was used to solve the gas phase without considering the effect of porosity. The equations for the gas-phase mass and its momentum conservation are respectively given by

$$\frac{\partial \varepsilon \rho}{\partial t} + \nabla \cdot \rho \varepsilon u = 0 \tag{9}$$

$$\frac{\partial \varepsilon \rho v}{\partial t} + \nabla \cdot \rho \varepsilon u v = -\nabla P + \nabla \cdot (\mu \varepsilon \nabla v) + \rho \varepsilon g - S \tag{10}$$

where, ρ is acceleration due to gravity, m/s^2; t is time, s; v is the volume of grid cell; μ is viscosity of the fluid (air), mm^3; ε is volume fraction of straw in the fluid (air); u is fluid (air) velocity, m/s; S is momentum sink; ∇ is vector symbol; P is momentum, kg·m/s.

The drag force is due to the relative motion of the gas and solid phases, and the coupling between these phases is obtained from the momentum sink S, which is given by

$$S = \frac{\sum_i^n F}{v} \tag{11}$$

where, F is fluid drag force acting on grid cell i of n total cells; v is volume of grid cell i of n total cells.

The particle model of the discrete element method simulates the particle-particle (boundary) contact using a vibration equation. This contact is decomposed into its tangential and normal directions with the respective vibration equations:

$$\begin{cases} \dfrac{m_{1,2}\mathrm{d}^2 u_n}{\mathrm{d}t^2} + \dfrac{c_n \mathrm{d}u_n}{\mathrm{d}t} + K_n u_n = F_n \\ \dfrac{m_{1,2}\mathrm{d}^2 u_s}{\mathrm{d}t^2} + \dfrac{c_s \mathrm{d}u_s}{\mathrm{d}t} + K_s u_s = F_s \\ \dfrac{I_{1,2}\mathrm{d}^2 \theta}{\mathrm{d}t^2} + \left(\dfrac{c_s \mathrm{d}u_s}{\mathrm{d}t} + K_s u_s\right) s = M \end{cases} \tag{12}$$

where, $m_{1,2}$ is equivalent mass of particles 1 and particles 2, g; $I_{1,2}$ is equivalent moment of inertia of particles 1 and 2, m^4; s is radius of rotation, mm; u_n and u_s are Displacements of the particles along the normal and tangential directions, respectively, mm; θ is rotation angle of the particle, (°); F_n and F_s are normal and tangential force components on the particle, respectively, N; M is external moment on the particle, N·m; K_n and K_s are normal and tangential elastic coefficients, respectively; c_n and c_s are normal and tangential damping coefficients, respectively.

The force on the particle can be calculated using Newton's second law of motion:

$$\begin{cases} m_i \ddot{u}_i = \sum F' \\ I_i \ddot{\theta}_i = \sum M \end{cases} \tag{13}$$

where, $\ddot{u}_i$ is acceleration of particle i; $\ddot{\theta}_i$ is angular velocity of particle i; m_i is mass of particle i; I_i is moment of inertia of particle i; $\sum F'$ is resultant external force acting on particle i at its center of mass; $\sum M$ is resultant external moment acting on particle i at its center of mass.

Apply the central difference to integrate Equation (5) and obtain the updated speed:

$$\begin{cases} (\dot{u}_i)_{N+\frac{1}{2}} = (\dot{u}_i)_{N-\frac{1}{2}} + \left[\sum F/m_i\right]_N \Delta t \\ \left(\dot{\theta}_i\right)_{N+\frac{1}{2}} = \left(\dot{\theta}_i\right)_{N-\frac{1}{2}} + \left[\sum F/I_i\right]_N \Delta t \end{cases} \tag{14}$$

where, Δt is time step; N is number of time steps corresponding to time t.

Integrate Equation (14) to obtain the following displacement equation:

$$\begin{cases} (u_i)_{N+1} = (u_i)_N + (u_i)_{N+\frac{1}{2}} \Delta t \\ (\theta_i)_{N+1} = (\theta_i)_N + \left(\dot{\theta}_i\right)_{N+\frac{1}{2}} \Delta t \end{cases} \tag{15}$$

The new displacement can then be obtained and substituted into the force displacement to update the force. Thus, the particle motion at any moment can be iteratively obtained.

Rice straw has various properties such as shearing, bending, and stretching. The high aspect ratio and anisotropy of such properties have hindered previous simulations of crushed straw. In addition, rice straw possesses strong tenacity, and once crushed, its tendency to coil causes agglomeration and entanglement.

Based on real scenarios, 7 mm diameter spheres spaced 3.5 mm center-to-center in an agglomeration or 100 mm long rod-shaped models were employed, shown in Figure 6, using the Hertz-Mindlin with bonding model in the EDEM software. The agglomerate and rod-shaped models were then filled into the large crushed straw model.

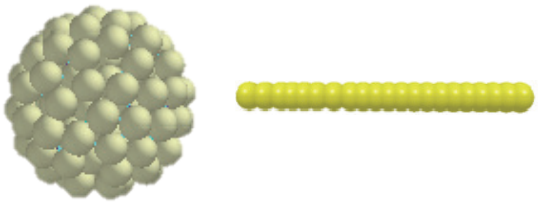

Figure 6 Straw model diagrams of agglomerate-shaped crushed straw and rod-shaped crushed straw

The material properties of each component and material of the planter determine the results obtained from the discrete element model. The parameters of the relevant material and contact mechanics were set as listed in Table 1 according to previous experiments.

Table 1 Material properties and related contact parameters for discrete element model

Parameter	Unit	Value
Straw density	kg·m^{-3}	241
Straw shear modulus	Pa	1×10^6
Straw Poisson's ratio	–	0.4
Straw density	kg·m^{-3}	7865
Steel shear modulus	Pa	7.9×10^{10}
Steel Poisson's ratio	–	0.3
Straw-steel recovery coefficient	–	0.3
Straw-steel static friction coefficient	–	0.6
Straw-steel rolling friction coefficient	–	0.01
Straw-stalk recovery coefficient	–	0.28

The gas-solid two-phase flow field was solved by coupling the FLUENT and EDEM software packages, and was calculated using the k-ε turbulence model. The airflow direction at the velocity inlet was set to follow the pipeline flow, and the airflow outlet was set as the pressure outlet. In the EDEM software, the step length was set to 5%, and the Hertz-Mindlin (no slip) collision model was used to model the interaction between the particles and pipeline wall[20-22].

4.2 Simulation and analysis

4.2.1 Motion of crushed straw in conveying device

Motion simulation diagram and velocity vector diagram of rice

straw in vane conveying device, as shown in Figures 7 and 8. It can be concluded from diagrams that crushed straw has high speed under the centrifugal force of the high-speed-rotation throwing blades and also the movement of agglomerate-shaped crushed straw and rod-shaped crushed straw. But motion velocity slows because of the pipeline's friction and collision. Farther research like coupling analysis is must.

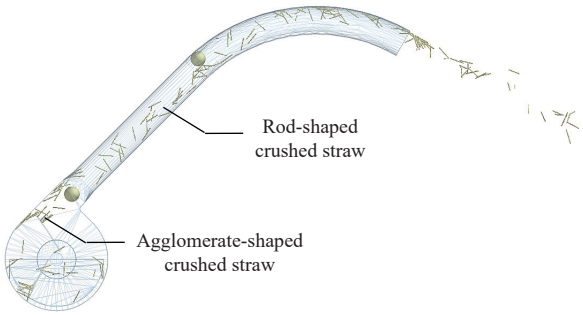

Figure 7 Motion simulation diagram of rice straw in vane conveying device

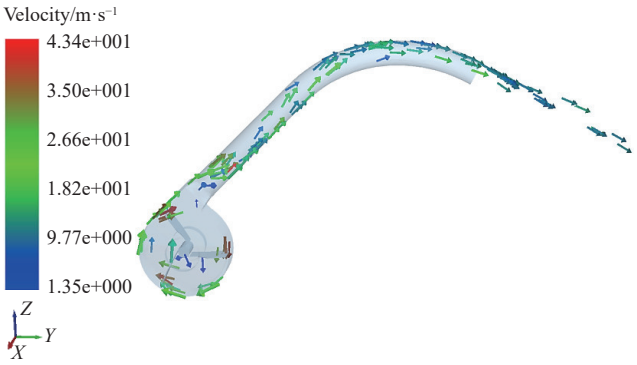

Figure 8 Velocity vector diagram of rice straw in vane conveying device

4.2.2 Flow field analysis

Figures 9 and 10 show the cloud diagrams of air velocity and gas-solid two-phase flow velocity, respectively. Under the action of the blade, the crushed straw entered the lifting pipeline at a relatively high initial speed similar to the linear velocity of the impeller. The airflow velocity on the upper wall of the pipeline was the highest in the straight pipeline section. The crushed straw was affected by the interaction of the airflow thrust, gravity, and friction, thus its motion was considerably affected by the complex characteristics of the flow field. In the elbow entrance section following the straight pipeline section, the strong collision against the curved wall surface immediately reduced the airflow speed, and the crushed straw changed its motion direction, as verified by the changing motion trend of particle concentration. The change was most apparent when the crushed straw first entered the elbow section. The highest particle concentration appeared close to the pipeline wall, and decreased with particle distance from the wall. The considerable crushed straw clogging at the exit of the elbow section can be observed to impede the smooth passage of air through the outer tube wall, creating a thick flow of crushed straw and slowing down the straw motion[23-25].

The results of the motion and flow field analyses of crushed straw in the conveying device indicate the pipeline environment should be designed to maintain a reasonable speed and a high material mobility to improve the conveying smoothness and prevent clogging while targeting a reasonable power consumption ratio.

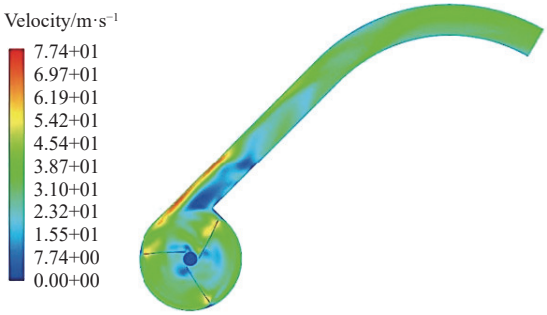

Figure 9 Air velocity result

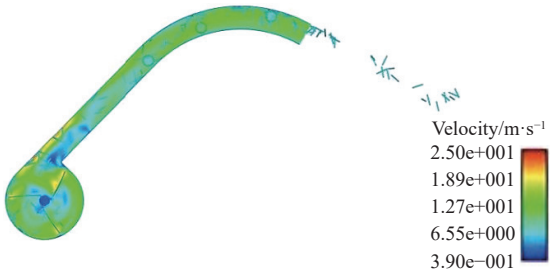

Figure 10 Gas-solid two-phase flow velocity cloud diagram

4.3 Effects of parameters on conveying device performance

According to the early stage operation and single-factor simulation test of the planter, suitable performance of the pipeline transportation can be fund.

In the motion simulation of crushed straw in the conveying device, parameter setting to the conveying straw volume 1.5 kg/s, pipeline diameter 210 mm. Considering the preliminary test results and real conditions, the simulations at throwing blade speeds of 1700, 1850, 2000, 2150, and 2300 r/min was executed. Figure 11a shows the speed of crushed straw under the five speeds. As the throwing blades become faster, the throwing speed of crushed straw increase. In addition, a higher speed implies a smoother transportation with higher fluidity and lower possibility of clogging. In the motion simulation of crushed straw in the conveying device, parameter setting to the throwing blade speed 2100 r/min, pipeline diameter 210 mm, and the conveying volume of crushed straw 1.3, 1.5, 1.7, 1.9, and 2.1 kg/s. Figure 11b shows the speed of crushed straw at the five conveying volumes. No notable change in the throwing speed of the crushed straw occurs at the different conveying volumes. But it can easily cause clogging at a conveying volume of 2.1 kg/s. In the motion simulation of crushed straw in the conveying device, the parameters were set as the conveying volume of crushed straw of 1.5 kg/s, throwing blade speed of 2100 r/min, and considering pipeline diameters of 180, 195, 210, 225, and 240 mm to simulate the straw motion. Figure 11c shows the speed of crushed straw at the fiveconveying volumes. Increasing the diameter of the pipeline increases the airflow and crushed straw speeds within the pipeline. Meanwhile, fluidity improves, rendering clogging unlikely.

Apart from the above kinematic analysis and flow field analysis, reduce specific power consumption is also important in practical work. Specific power consumption reflected the value of power consumption, throwing blade speed reflected the working smoothly. Therefore, by comprehensively considering the need for high planter operation efficiency and the optimal power consumption, the highest throwing speed of crushed straw and lowest specific power consumption are required, field test evaluation is must.

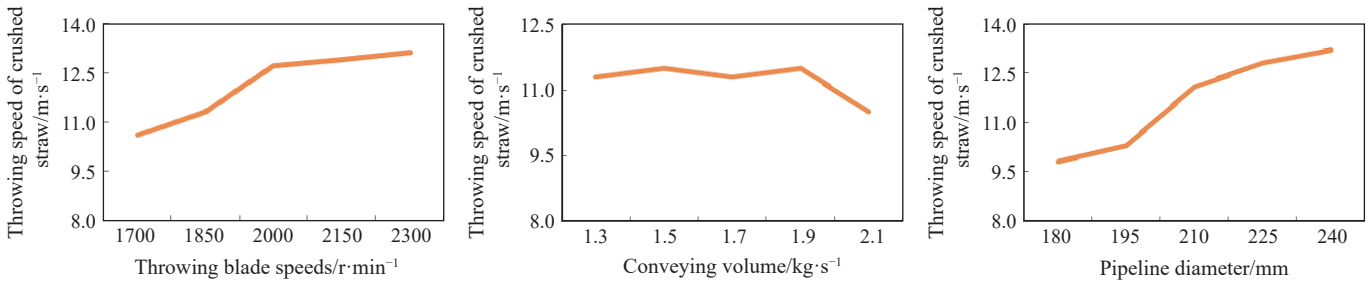

a. Effect of throwing blade speed on conveying performance

b. Effect of conveying volume on conveying performance

c. Effect of pipeline diameter on conveying performance

Figure 11 Simulation results of different single-factors on peed of straw

5 Field test evaluation

5.1 Experimental setup

Based on the simulation results and real planter operation, the field experiment was conducted using a prototype of the throwing device in a rice field after harvest at the Liuhe Experimental Base of the Jiangsu Academy of Agricultural Sciences. The prototype had a working width of 2.2 m and moved at a forward speed of 0.7 m/s. Its components included the crushed straw throwing and lifting device with adjustable-speed blades, the horizontal-level conveying device with adjustable feed rate, and easily replaceable conveying pipelines.

The conveyed crushed straw was recorded using a HiSpec5 high-speed camera (Fastec Imaging, San Diego, CA, USA; HiSpec2Director control software; ProAnalyst Professional 2D video processing software; 1376×1132 pixels resolution; 200 fps sampling rate; and 4998 μs exposure time) at different throwing speeds under various operating conditions. The throwing speeds were then analyzed through video processing. The experimental scenario is shown in Figure 12.

Figure 12 Experimental scenario to verify crushed straw throwing

By considering the planter structure and operation analysis, especially the preliminary tests of the research team, the values should be controlled within a reasonable range. The test parameters and their values are listed in Table 2, establishing a three-factor, three-level test design[26-28]. The throwing speed of the crushed straw was defined as Y_1 (i.e., straw speed achieved after throwing-lifting, pneumatic crossing, and wall-pressure jetting), and the specific power consumption Y_2 was defined as the evaluation index of the pipeline transportation performance. Subsequently, the experiments were performed by varying the throwing blade speed X_1, conveying volume of crushed straw X_2, and pipeline diameter X_3[29,30]. The torque and revolution speed sensor is shown in Figure 13.

The specific power consumption Y_2 can be calculated as follows:

$$Y_2 = \frac{P_j - P_q}{Q} \tag{16}$$

where, P_j is power consumption of cleaning and conveying device, W; P_q is power consumption excluding the cleaning and conveying device, W; Q is conveying volume of crushed straw, kg/s.

Table 2 Test factor levels

Level	Throwing blade speed X_1/r·min^{-1}	Conveying volume of crushed straw X_2/kg·s^{-1}	Pipeline diameter X_3/mm
−1	1700	1.3	200
0	2000	1.6	220
1	2300	1.9	240

Figure 13 Torque and revolution speed sensor

5.2 Results and discussion

The three-factor, three-level test was analyzed using the Box-Behnken experiment design in the Design-Expert software to perform quadratic polynomial regression on the test data and applied a response surface analysis to study the correlation of various factors as well as the law of influence for the interaction effects. The test conditions and results are listed in Table 3.

Table 3 Test conditions and results

Test No.	X_1	X_2	X_3	Y_1/m·s^{-1}	Y_2/(×10^3 m^2·s^{-2})
1	0	−1	−1	10.9	6.5
2	0	0	0	12.7	12.2
3	0	−1	1	12.5	13.2
4	0	1	−1	11.1	14.5
5	1	−1	0	12.6	10.8
6	0	0	0	12.8	11.6
7	0	0	0	12.6	11.5
8	0	0	0	12.9	11.9
9	1	0	1	14.6	18.5
10	0	1	1	11.6	17.8
11	1	1	0	12.4	16.8
12	−1	−1	0	10.1	5.5
13	1	0	−1	13.3	16.1
14	−1	1	0	10.1	9.9
15	−1	0	1	11.9	12.4
16	0	0	0	12.8	12.4
17	−1	0	−1	11.2	8.2

Note: The test conditions as defined in Table 2; Y_1 is the throwing speed of crushed straw and Y_2 is specific power consumption.

Based on the data in Table 2, Design-Expert was used to conduct a multiple regression fitting and thereby determine the optimal operation parameters. A second-order polynomial response surface regression model between the three independent variables was established. The effect of throwing blade speed X_1, conveying volume of crushed straw X_2, and pipeline diameter X_3 on the throwing speed of crushed straw Y_1 and specific power consumption Y_2 were investigated in this study. The significance values resulting from this regression analysis are listed in Table 4. According to these results, research team obtained a response surface diagram describing the influences of the interactions between each independent variable on the response variable, as shown in Figures 14-16.

Table 4 Significance test results

Source of variation	Y_1				Y_2			
	Sum of squares	df	F	p-value	Sum of squares	df	F	p-value
Model	21.87	9	201.27	<0.0001	211.98	9	54.18	<0.0001
X_1	11.52	1	954.32	<0.0001	85.81	1	197.38	<0.0001
X_2	0.1013	1	8.39	0.0231	66.13	1	152.11	<0.0001
X_3	2.10	1	174.07	<0.0001	34.44	1	79.24	<0.0001
X_1X_2	0.0100	1	0.8284	0.3930	0.6400	1	1.47	0.2643
X_1X_3	0.0900	1	7.46	0.0293	0.8100	1	1.86	0.2145
X_2X_3	0.3025	1	25.06	0.0016	2.89	1	6.65	0.0366
X_1^2	0.0581	1	4.82	0.0643	0.1441	1	0.3315	0.5828
X_2^2	7.59	1	628.65	<0.0001	4.09	1	9.40	0.0182
X_3^2	0.0487	1	4.03	0.0847	17.95	1	41.30	0.0004
Residual	0.0845	1			3.04	7		
Lack of fit	0.0325	3	0.8333	0.5413	2.45	3	5.57	0.0653
Error	0.0520	4			0.5880	4		
Cor Total	21.95	16			215.02	16		

Note: p≤0.001, highly significant; p≤0.05, significant; p>0.1 not significant.

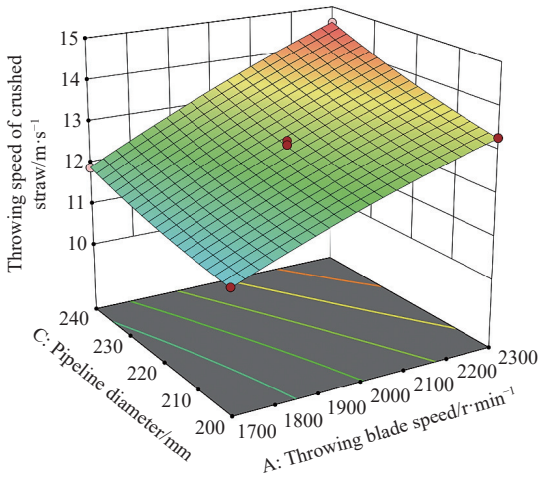

Figure 14 Influence of the speed of the throwing blade and pipe diameter on the throwing speed of crushed straw

From Table 4, it can be observed that for throwing speed of crushed straw model and specific power consumption model, value of p<0.0001 respectively indicates a high significance, and for the lack of fit, values of p>0.05 indicates that the regression equation had a high degree of fit. Therefore, the throwing speed model and specific power consumption model can be used to optimize the operation parameters of the crushed straw lifting and throwing device in the uniform crushed straw throwing and seed-sowing machine.

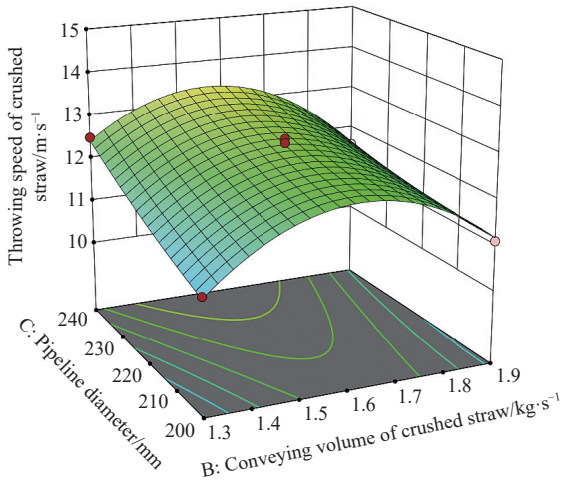

Figure 15 Influence of conveying volume of crushed straw and pipe diameter on the throwing speed of crushed straw

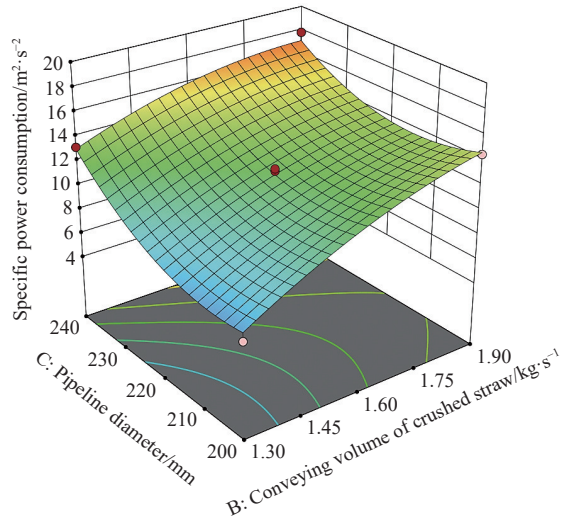

Figure 16 Influence of pipe diameter and conveying volume of crushed straw on specific power consumption

In model Y_1 of the crushed straw throwing speed, three regression variables, X_1, X_3, and X_2^2, were highly significant (p<0.001), and X_2, X_1X_3, and X_2X_3 were significant (p<0.05); none of the remaining conditions were significant. In model Y_2 of specific power consumption, three regression variables, X_1, X_2, and X_3 were highly significant (p<0.001), and X_2X_3, X_2^2, and X_3^2 were significant (p<0.05); none of the remaining conditions were significant.

The test results indicated that, during lifting and throwing, a higher throwing blade rotational speed improved the conveying performance in the pipeline, increasing the throwing speed and specific power consumption. In addition, a larger pipeline diameter provided a smoother motion of the crushed straw and reduced congestion while also increasing the straw throwing speed and specific power consumption. In contrast, an excessively high conveying volume leads to clogging, whereas a very small conveying volume can lower the throwing speed and reduce operational efficiency. So the specific power consumption would at first decrease and then increase as conveying volume increase.

Therefore, this study therefore obtained the optimal parameters for the planter device operation by neglecting non-significant regression variables, and optimized model Y_1 and Y_2 to obtain the following regression equation:

$$Y_1 = 12.76 + 1.2X_1 - 0.1125X_2 + 0.5125X_3 + 0.15X_1X_3 - 0.275X_2X_3 - 1.34X_2^2 \quad (17)$$

$$Y_2 = 11.84 + 3.28X_1 + 2.88X_2 + 2.08X_3 - 0.85X_2X_3 - 0.9947X_2^2 + 2.06X_3^2 \quad (18)$$

The test results indicated that to obtain a higher throwing speed, the pipeline wind speed and pipeline diameter must be increased and the conveying volume optimized accordingly, at the expense of obtaining a lower specific power consumption. Therefore, by comprehensively considering the need for high planter operation efficiency and the optimal power consumption, the highest throwing speed of crushed straw and lowest specific power consumption are required. This problem was solved using the Design-expert software.

The results of optimization shows that the predict the best optimal parameters were 2000 r/min throwing blade rotational speed, 1.4 kg/s conveying volume, and 220 mm pipeline diameter, the planter achieved a throwing speed of 12.2 m/s and specific power consumption of 9179 m^2/s^2.

5.3 Field verification tests

After adjusting the structural and operating parameters of the planter straw-crushing mechanism, horizontal-level straw conveying device, and crushed straw lifting and throwing device, the field test verification was conducted.

The tests had been repeated for three times on the field by using the optimization results and the results were averaged. Figure 17 shows the test verification scenario and uniform throwing results. Test area was in Nanjing Institute of Agricultural Mechanization, Ministry of Agriculture and Rural Affairs, the planter achieved a throwing speed 12.4 m/s and specific power consumption 9070 m^2/s^2 while the best optimal parameters were 2000 r/min throwing blade rotational speed, 1.4 kg/s conveying volume, and 220 mm pipeline.

Figure 17 Field verification test of uniform-throwing planter

Either of the relative errors between the experimental and predicted values of specific power consumption and throwing speed are small, which indicated a reasonable choice of optimization conditions. Thus, the optimal parameters can provide a high-performance operation that satisfies standards for field application under the determined optimal parameters. Compared to previous test, the specific power consumption is clearly reduced, the throwing speed is obviously increased, and the performance of uniform crushed straw throwing and seed-sowing machine has been greatly improved. All operation quality can meet the relevant agricultural machinery industry technical standards and local production agronomic requirements, indicating the uniform crushed straw throwing and seed-sowing machine with optimized key structural parameters had better working performance, which would provide theoretical basis and technical reference for achieving the high-quality and smooth compound operation.

6 Conclusions

In this study, the research team explored an uniform crushed straw throwing and seed-sowing machine. As rice straw is massive and has a high moisture content, high tenacity, and tendency to entangle and agglomerate once crushed, we first analyzed the kinematic and dynamic characteristics of uniform crossways throwing of crushed straw. A particle motion simulation was adopted based on a CFD-DEM model to conduct a gas-solid coupling analysis. By constructing and analyzing the rigid-flexible coupling and the corresponding interactions, a theoretical formulation and basis for simulation analysis to optimize the planter structural and motion parameters was provided.

Subsequently, the pipeline conveying performance was simulated under different operating conditions considering three parameters: throwing blade speed, crushed straw conveying volume, and pipeline. The analysis focused on the resulting smoothness of the conveying and throwing speed, as well as specific power consumption.

Based on the simulation results and real planter operation, we conducted a field experiment and applied a response surface analysis to study the correlation of various factors as well as the law of influence for the interaction effects.

A second-order polynomial response surface regression model between the three independent variables was established. The effect of throwing blade speed X_1, conveying volume of crushed straw X_2, and pipeline diameter X_3 on the throwing speed of crushed straw Y_1 and specific power consumption Y_2 were investigated in this study. The highest throwing speed of crushed straw and lowest specific power consumption are the optimization goal.

The results of optimization shows that the predict the best optimal parameters were 2000 r/min throwing blade rotational speed, 1.4 kg/s conveying volume, and 220 mm pipeline diameter, the planter achieved a throwing speed of 12.2 m/s and specific power consumption of 9179 m^2/s^2. And then the field test verification was conducted. The planter achieved a throwing speed 12.4 m/s and specific power consumption 9070 m^2/s^2 while selecting the best optimal parameters .Thus, the optimal parameters can provide a high-performance operation that satisfies standards for field application under the determined optimal parameters, satisfying the actual operation requirements and providing support for optimal planter design and parameter setting.

Acknowledgements

This work was supported by the earmarked fund for CARS-13; Natural Science Foundation of Jiangsu Province (Grant No. BK20221187).

[References]

[1] Hu Z C. Great breakthrough in the research and development of the mechanical no-tillage planter technology in full straw mulching field. Prim. Agr. Technol. Extn., 2015; 4: 40.

[2] Bagnall G, Thomasson J, Ge Y. Ani mal drawn conservation tillage planter designed for small farms in the developing world. Appl. Eng. Agri., 2016; 32(6): 791–799.

[3] Liu F. Study on cultivation mode of no tillage direct seeding rapeseed *Brassica napus* L.) based on rich straw mulching. Wuhan: Huazhong Agricultural University, 2012. (in Chinese)

[4] Chen Y, Wu F, Gu F, Wang B, Ma B, Hu Z. Test on peanut no-till planter under the coverage of the wheat straw. J. Chin. Agr. Mechanization, 2014; 35(2): 132–135. (in Chinese)

[5] He J, Li H W, Chen H T, Lu C Y, Wang Q J. Research progress of

conservation tillage technology and machine. Transactions of the CSAM, 2018; 49(4): 1–19. (in Chinese)
[6] Matin M A, Desbiolles J M A, Fielke J M. Strip-tillage using rotating straight blades: Effect of cutting-edge geometry on furrow parameters. Soil & Tillage Research, 2016; 155(8): 271–279.
[7] Matin M A, Fielke J M, Desbiolles J M A. Torque and energy characteristics for strip-tillage cultivation when cutting furrows using three designs of rotary blade. Biosystems Engineering, 2015; 129(1): 329–340.
[8] Sidhu H S, Singh M, Singh Y, Blackwell J, Lohan S K, Humphreys E, et al. Development and evaluation of the turbo happ.seeder for sowing wheat into heavy rice residues in NW India. Field Crops Research, 2015; 184(7): 201–212.
[9] Elfatih A, Arif E M, Atef A E. Evaluate the modified chopper for rice straw composting. Journal of Applied Sciences Research, 2010; 6(8): 1125–1131.
[10] Shi Y Y, Sun X R, Wang X C, Hu Z C, David N, Ding W M. Numerical simulation and field tests of minimum-tillage planter with straw smashing and strip laying based on EDEM software. Computers and Electronics in Agriculture, 2019; 166: 1–10.
[11] Shi Y Y, Luo W W, Hu Z C, Wu F, Gu F W, Chen Y Q. Design and test of equipment for straw crushing with strip-laying and seed-belt classification with cleaning under full straw mulching. Transactions of the CSAM, 2019; 50(4): 58–67. (in Chinese)
[12] Gu F W, Gao X M, Wu F, Hu Z C, Chen Y Q, Zhang C. Improvement of uniform scattering device for straw-smashing, back-throwing, no-tillage planter under complete straw mulching condition. Int J Agric & Biol Eng, 2018; 11(6): 49–57.
[13] Shi Y Y, Wang X C, Hu Z C, Gu F W, Wu F, Chen Y Q. Optimization and experiment on key structural parameters of no-tillage planter with straw-smashing and strip-mulching. Int J Agric & Biol Eng, 2021; 14(3): 103–111.
[14] Xu H B, Hu Z C, Wu F, Gu F W, Chen Y Q. Design of straw distributed retention device of wheat planter under full rice straw retention. Transactions of the CSAE, 2019; 35(9): 19–28. (in Chinese)
[15] Gu F W, Hu Z C, Chen Y Q, Wu F. Development and experiment of peanut no-till planter under full wheat straw mulching based on 'clean area planting'. Transactions of the CSAE, 2016; 32(20): 15–23. (in Chinese)
[16] Luo W W, Hu Z C, Wu F, Gu F W, Xu H B, Chen Y Q. Design and optimization for smashed straw guide device of wheat clean area planter under full straw field. Transactions of the CSAE, 2019; 35(18): 1–10. (in Chinese)
[17] Liu Y F, Lin J, Hao B Y. Design and experiment of testing device for soil working tool in no-tillage planter. Transactions of the CSAE, 2016; 32(17): 24–31. (in Chinese)
[18] Tian Y, Lin J, Li B F. Design and test of conveying device of pneumatic straw deep burying and returning machine. Transactions of the CSAE, 2018; 49(12): 36–44.
[19] Zhai Z P, Yang Y Y, Gao B. Power consumption and parameter optimization of stalk impeller blowers. Transactions of the CSAE, 2013; 29(10): 26–33. (in Chinese)
[20] Gao B. Analysis of flow within an impeller blower. PhD dissertation. Huhhot: Inner Mongolia University of Technology, 2013; 57p. (in Chinese)
[21] Fang H M. Research on the straw-soil-rotary blade interaction using discrete element method. PhD dissertation. Nanjing: Nanjing Agricultural University, 2016; 121p. (in Chinese)
[22] Liao Q X. Experimental study on anti-blocking and metering mechanism of no-till planter. PhD dissertation. Beijing: China Agricultural University, 2013; 120p. (in Chinese)
[23] Zhang C Y, Ma C, Yan F. Gas solid two phase flow characteristics of elbow pipe with different bending radius ratio based on the CFD-DEM method. Journal of Jiangsu University of Science and Technology (Natural Science Edition), 2018; 171(6): 803–808. (in Chinese)
[24] Krzysztof S, Aleksander L. Two-stage motion of particles in the discharge spout of forage harvester. Agricultural Engineering, 2010; 124(6): 245–252.
[25] Lisowsk N. Movement of chopped material in the discharge spout of forage harvester with a flywheel chopping unit: Measurements using maize and numerical simulation. Biosystems Engineering, 2012; 111(4): 381–391.
[26] NY/T500-2015. Operation quality of smashed straw machine. (in Chinese)
[27] Lü J, Shang Q, Yang Y, Li Z, Li J, Liu Z. Performance analysis and experiment on granular fertilizer spreader with cone disc. Transactions of CSAE, 2016; 32(11): 16–24. (in Chinese)
[28] McGrath D, Smith C, Gholz H, Oliveira F. Effects of land-use change on soil nutrient dynamics in Amazonia. Ecosystems, 2001; 4(7): 625–645.
[29] Zhai Z P, Wang C G. Numerical simulation and optimization for air flow in an impeller blower. Transactions of the CSAM. 2008; 39(6): 84–87. (in Chinese)
[30] Liu F Y. Discrete element modelling of the wheat particles and short straw in cleaning devices. PhD dissertation. Xianyang: Northwest A&F University, 2018; 127p. (in Chinese)